



Scientific- Research Article

Sliding Mode Stabilization of Quad Tilt-wing UAV Considering Nonlinear Model of the Vehicle and Uncertainties

M. Amani Estalkhkuhi^{1*}, J. Roshanian²

1-2- Department of Aerospace Engineering, K. N. Toosi University of Technology, Tehran, Iran

ABSTRACT

Keywords: *Quadrotor UAV, VTOL, Morphing wing, MIMO systems, Robust control.*

In this paper, a multi-input/multi-output sliding controller is proposed and analyzed for a quad tilt-wing unmanned aerial vehicle (QTW-UAV). The vehicle is equipped to do take-off and landing in vertical flight mode and is capable of flight over long distances in horizontal flight mode. The full dynamic model of the vehicle is originated from the Newton-Euler formulation. For developing the controller, a set of integral type sliding surfaces is selected and it is necessary to mention that in this approach, there is no linearization during controller design. Simulation has been conducted for a nonlinear, multivariable model that includes uncertain parameters and in the presence of pitch angle measurement noise and pitch moment disturbance. For verification, the proposed controller is compared with linear based controller design simulation. Results exhibit that the proposed controller is robust in the face of uncertainties, noise, and disturbance and meets performance demands with control inputs of low amplitude.

Nomenclature

m	Mass	ρ	Air density
I	Identity matrix	A	Area of wing
J_b	Diagonal inertia matrix	J_{prop}	Rotor rotational inertia
V_i	Linear velocity in the inertial frame	T_i	Rotor reaction torque
Ω_b	Angular velocity in the body frame	M	Inertia matrix
$F_{(\cdot)}$	Force	C	Coriolis-centripetal matrix
$M_{(\cdot)}$	Moment	u_i	Control commands
$R_{(\cdot)}$	Rotational matrix	p, q, r	Angular velocity about axis
g	Gravity acceleration	ϕ, θ, ψ	Euler angles
α_i	Effective angle of attack	X, Y, Z	Positions
Θ	Tilt angle	S	Sliding surface
ω_i	Rotor rotational speed	e	Error
$V_{(\cdot)}$	Velocity	Φ	Sliding boundary layer
C_D	Drag coefficient	Δ	Variance
C_L	Lift coefficient		

1 Msc (Corresponding Author) **Email:** * amani@kntu.ac.ir

2 Professor

DOI: [10.22034/jast.2022.296063.1086](https://doi.org/10.22034/jast.2022.296063.1086)

Submit: 31.07.2021/ Accepted: 09.01.2022

Print ISSN:1735-2134 Online ISSN: 2345-3648

Introduction

Due to the development of fly robots in the last decade, their participation in urban and non-urban services has increased, for example, remote sensing services in precision agriculture, forest health monitoring, air traffic control, mapping [1], borders security [2], traffic surveillance [3], power line monitoring [4], parcel delivery [5], aerial attack, etc. Furthermore, indoor missions like imaging, search and rescue among the tasks that are assigned to them.

To accomplish these missions, the drones are used. Unmanned Aerial Vehicles (UAV) can be categorized in terms of wing structure into two main classes: fixed-wing UAVs, and rotary-wing UAVs, and each type has its own advantages and drawbacks [6]. Fixed-wing UAVs have high cruising speed and altitude. They can fly as the long-range endurance and are able to carry heavy payload because of their large cabin capacity. However, requiring some equipment and runway for take-off and landing are restrictions of fixed-wing UAVs.

Rotary-wing UAVs, on the other hand, can vertically take-off and land (VTOL) without any required substructure. Also, they do not require any airflow for maneuvering. But they have lower speeds and range of flight.

Morphing technology can now combine these advantages by a hybrid design of the wing. In the tree diagram of the morphing technology illustrated in Figure 1, there are several techniques for the hybrid wing design of an aircraft such as survey of a wing-sweep morphing aircraft [7], Albatrosses biologically inspired morphing in shape as sweep and size as span extension [8], bionic bird wing-foldable UAV [9], Z-shaped morphing-wing [10], etc., but among these techniques, we deal with the rotation of the whole wing in incidence. This configuration is in the subdirectory of the rotating wing named tilt-wing. This hybrid design combines the vertical flight capabilities of rotary-wing UAVs with the high-speed cruise flight of fixed-wing UAVs. Given all the benefits of this design, there are disadvantages such as the high complexity of the vehicle's dynamics and the cost and the weight of the hinge and the rotation equipment.

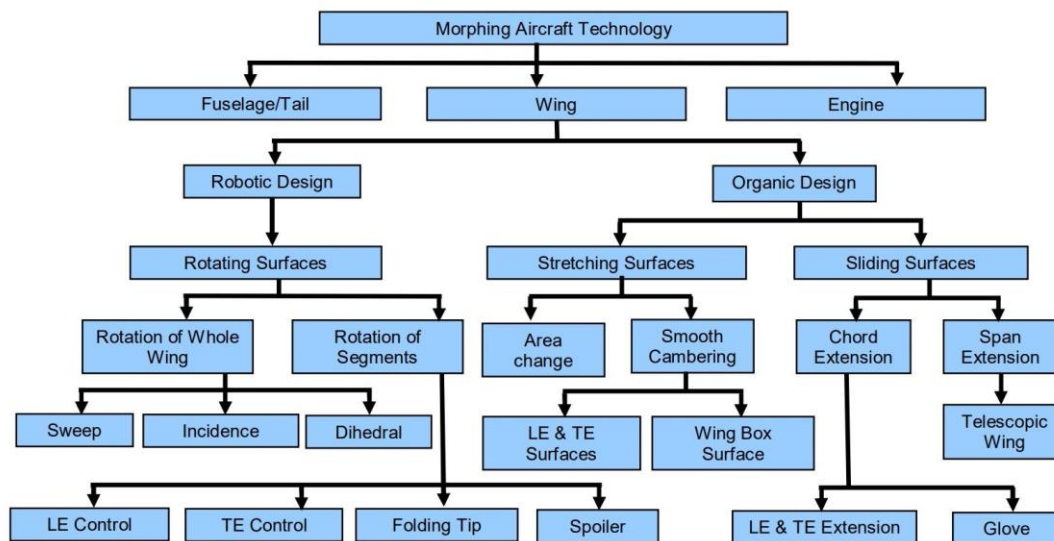


Figure 1: Categorization of morphing aircraft technology [11].

There are several designs in the tilt-wing category such as new-style distributed propulsion tilt-wing UAV [12], albatross-inspired tilt-wing UAV [8], [13], tilt-wing rotorcraft [14], single tilt-wing [15], tilt-wing aircraft [16], A³ Vahana VTOL tilt-wing [17], etc. In this paper, among different configuration designs of the tilt-wing, the quad tilt-wing (QTW) is selected as the baseline (see Figure 2). In the selected configuration, there are four

rotors on the leading edges of four wings with ability to tilt about their transverse axes. Despite the complexity and difficult control of QTW, there has been an extensive research on this field in recent years.

Some of these research focused on the aerodynamic characteristics and design [18], [19], other studies such as [20], configured Kalman filter-based linear quadratic integral (LQI) control method, and [21] designed an LQR and SMC with

recursive implementation, which for LQR the dynamic equations of the vehicle are linearized around nominal operating points in hovering condition. In [22], [23] robust hovering and position PID type controllers on linear dynamical model under modeled aerodynamic disturbances are developed. Moreover, the studies [24], [25], focused on design and developed a novel quad tilt-wing and analyzed it with hierarchical control system design. Also, [26] applied a PID controller on Sabanci University Unmanned Aerial Vehicle (SUAVI). Several studies work on Stability Augmentation System (SAS) and gain-scheduled flight controller of the QTW, e.g. [27]–[29]. Hierarchical adaptive control approach is considered in [30], [31]. The dynamic inversion method, which is a linearization method without an approximation algorithm is clarified in [32]. The research series [33]–[35], studied the stability and control augmentation system (SAS and CAS). Linear Quadratic Gaussian (LQG) control design on a nonlinear dynamical model in the presence of aerodynamic disturbances is developed in [36]. Further, from former authors a Model Predictive Control (MPC) design is expressed in another study [37] and an advanced Computer Aided Design (CAD) methodology for Processor-In-the-Loop (PIL) co-simulation and rapid control prototyping of a QTW is stated in [38]. In studies [39] and [40] a fuzzy Gain-Scheduled Proportional-Integral-Derivative (GS-PID) and a Linear Quadratic Gaussian (LQG) controller are configured, respectively. And recent studies, used Dynamic Inversion (DI), this is one example of the linearization method suggested for the UAVs proposed in [41], and an H_∞ controller applied to dynamical model linearized QTW by Dynamic Inversion (DI) method is suggested in study [42]. The above-mentioned studies showed promising successful results. However, some of them use linearization or approximation in vehicle model or control development process and do not analyze the simulation in the presence of uncertainties. In this study, a multi-input/multi-output SMC is presented without any linearization in design process nor any approximation in the modeling of QTW. This control approach is acceptable in amplitude of control signals in the presence of modeling imprecision. To show the necessity of using a controller based on nonlinear model, a SMC controller with respect to linear model is conducted on the nonlinear model and its results in the presence of uncertainties, sensor noise, and

aerodynamic perturbations are compared with the results of the main control design.

This paper is organized as follows: In Section 2, the model of an aerial vehicle considering nonlinearities is provided. The flight controller of aerial vehicle is designed in Section 3. Simulation results are presented in Section 4, and finally, a conclusion and some future work are drawn in Section 5.

System Model

The aerial vehicle's nonlinear 6 DOF equations of motion including 3 DOF equations in transitional motion and 3 DOF equations in rotational motion are derived using Newton-Euler formulation. For a general unmanned aerial vehicle system, the equations of motion assuming that the vehicle is a rigid body can be written as

$$\begin{bmatrix} mI & 0 \\ 0 & I_b \end{bmatrix} \begin{bmatrix} \dot{V}_i \\ \dot{\Omega}_b \end{bmatrix} + \begin{bmatrix} 0 \\ \Omega_b \times (I_b \Omega_b) \end{bmatrix} = \begin{bmatrix} F_t \\ M_t \end{bmatrix} \quad (1)$$

Where the subscripts used as b and i represent the quantities in body and inertial frames, respectively. m , I , and 0 denote the mass, identity, and zero 3×3 matrices, respectively. Also I_b implies the diagonal inertia matrix of the UAV in the body frame. The linear velocity in the inertial frame and the angular velocity in the body frame of the UAV are represented by V_i and Ω_b , respectively. The left hand side of (1) is standard for many aerial vehicles; however, the net force and the moment terms, F_t and M_t , are case dependent (Figure 2).

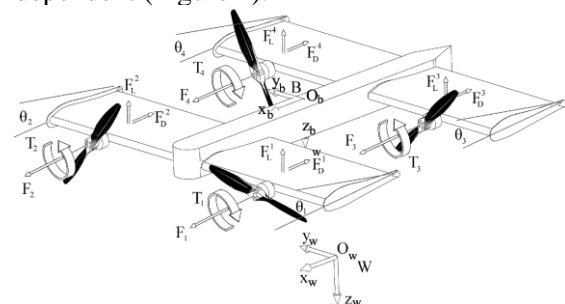


Figure 2: The forces and moments that act on the vehicle [25].

It should be pointed out that for tilt-wing quadrotors, the net external force F_t is composed of the gravity force on the vehicle F_{grav} , motor thrusts F_{thru} , aerodynamic forces applied on the wings and the fuselage F_{aero} and external disturbances like winds and gusts F_{dist} . These sources of force are functions of the effective wing angle of attacks (Figure 3). It must be stated that the forces are distributed in the body coordinate

frame and it is desired to be transformed to inertial frame distribution via the rotational matrix R_{b2i} as follows:

$$F_t = R_{b2i}(F_{grav} + F_{thru} + F_{aero} + F_{dist}) \quad (2)$$

Where,

$$R_{b2i} = \begin{bmatrix} c_\psi c_\theta & s_\phi s_\theta c_\psi - c_\phi s_\psi & c_\phi s_\theta c_\psi + s_\phi s_\psi \\ s_\psi c_\theta & s_\phi s_\theta s_\psi + c_\phi c_\psi & c_\phi s_\theta s_\psi - s_\phi c_\psi \\ -s_\theta & s_\phi c_\theta & c_\phi c_\theta \end{bmatrix} \quad (3)$$

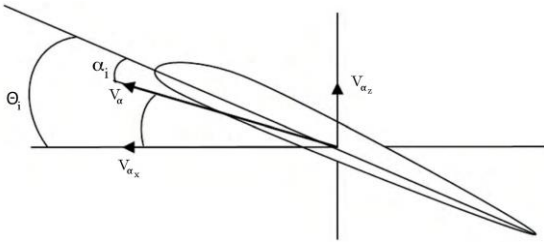


Figure 3: Effective angle of attack α_i ; $i = 1, 2, 3, 4$.

$$F_{grav} = \begin{bmatrix} -s_\theta \\ s_\phi c_\theta \\ c_\phi c_\theta \end{bmatrix} mg \quad (4)$$

$$F_{thru} = \begin{bmatrix} c_{\theta_1} & c_{\theta_2} & c_{\theta_3} & c_{\theta_4} \\ 0 & 0 & 0 & 0 \\ -s_{\theta_1} & -s_{\theta_2} & -s_{\theta_3} & -s_{\theta_4} \end{bmatrix} \begin{bmatrix} k\omega_1^2 \\ k\omega_2^2 \\ k\omega_3^2 \\ k\omega_4^2 \end{bmatrix} \quad (5)$$

And

$$F_{aero} = \begin{bmatrix} F_{aero_x} \\ F_{aero_y} \\ F_{aero_z} \end{bmatrix} = \begin{bmatrix} F_{D_1} + F_{D_2} + F_{D_3} + F_{D_4} \\ 0 \\ F_{L_1} + F_{L_2} + F_{L_3} + F_{L_4} \end{bmatrix} \quad (6)$$

In these equations, c_{θ} and s_{θ} imply $\cos(\theta)$ and $\sin(\theta)$, respectively. θ_i ($i = 1, 2, 3, 4$) denotes the wing tilt angle with regard to the x body axis. It should be emphasized that the motor thrusts are modeled as $k\omega_i^2$, where the rotor rotational speed notation is as ω_i .

It is important to note that the lift and drag forces are expressed in the wind frame and have to be transformed via rotational matrix with respect to effective angle of attack as R_{w2b} . Where w expresses the quantities in the wind frame.

$$R_{b2w} = \begin{bmatrix} c_{\alpha_i} & s_{\alpha_i} & 0 \\ -s_{\alpha_i} & c_{\alpha_i} & 0 \\ 0 & 0 & 1 \end{bmatrix} \quad (7)$$

That

$$\alpha_i = \theta_i - (-\arctan2(V_{\alpha_z}, V_{\alpha_x})) \quad (8)$$

It is obvious that

$$R_{w2b} = (R_{b2w})^{-1} \quad (9)$$

so with respect to (7) and (9), forces can be written as:

$$\begin{bmatrix} F_{D_i} \\ 0 \\ F_{L_i} \end{bmatrix} = R_{w2b} \begin{bmatrix} -\frac{1}{2} C_D \rho A V_\alpha^2 \\ 0 \\ -\frac{1}{2} C_L \rho A V_\alpha^2 \end{bmatrix} \quad (10)$$

That

$$V_\alpha = \sqrt{V_{\alpha_x}^2 + V_{\alpha_z}^2} \quad (11)$$

in the equation (10), C_D , and C_L are aerodynamics coefficient of drag and lift, respectively. Also ρ is the air density, A is the platform area of wing and V_α is the airflow velocity.

The total moment M_t consists of the moments created by the propellers gyroscopic effects M_{gyro} , the moments made by the rotors M_{thru} , aerodynamic forces M_{aero} and finally torques due to external disturbances M_{dist} .

$$M_t = M_{gyro} + M_{thru} + M_{aero} + M_{dist} \quad (12)$$

Where,

$$M_{gyro} = \sum_{i=1}^4 \left(J_{prop} \left[\eta_i \Omega_b \times \begin{bmatrix} c_{\theta_i} \\ 0 \\ -s_{\theta_i} \end{bmatrix} \omega_i \right] \right) \quad (13)$$

$$M_{thru} = l_s \begin{bmatrix} s_{\theta_1} - \frac{\lambda_1}{l_s} c_{\theta_1} & -s_{\theta_2} - \frac{\lambda_2}{l_s} c_{\theta_2} & s_{\theta_3} - \frac{\lambda_3}{l_s} c_{\theta_3} & -s_{\theta_4} - \frac{\lambda_4}{l_s} c_{\theta_4} \\ \frac{l_l}{l_s} s_{\theta_1} & \frac{l_l}{l_s} s_{\theta_2} & -\frac{l_l}{l_s} s_{\theta_3} & -\frac{l_l}{l_s} s_{\theta_4} \\ c_{\theta_1} + \frac{\lambda_1}{l_s} s_{\theta_1} & -c_{\theta_2} + \frac{\lambda_2}{l_s} s_{\theta_2} & c_{\theta_3} + \frac{\lambda_3}{l_s} s_{\theta_3} & -c_{\theta_4} + \frac{\lambda_4}{l_s} s_{\theta_4} \end{bmatrix} \times \begin{bmatrix} k\omega_1^2 \\ k\omega_2^2 \\ k\omega_3^2 \\ k\omega_4^2 \end{bmatrix} \quad (14)$$

And

$$M_{aero} = \begin{bmatrix} M_{aero_x} \\ M_{aero_y} \\ M_{aero_z} \end{bmatrix} = \begin{bmatrix} l_s (F_{L_1} - F_{L_2} + F_{L_3} - F_{L_4}) \\ l_l (F_{L_1} + F_{L_2} - F_{L_3} - F_{L_4}) \\ l_s (-F_{D_1} + F_{D_2} - F_{D_3} + F_{D_4}) \end{bmatrix} \quad (15)$$

In these expressions, J_{prop} is the rotational inertia of the rotors about their rotational axes, η_i is the sign of rotors rotation that is equal to 1, -1, -1, 1 for rotor numbers 1,2,3, and 4, respectively (see Figure 2). l_s and l_l indicate the span-wise and longitudinal distances between the rotor axes and mass center of vehicle, respectively. Furthermore, the rotor reaction torques are considered as $T_i = \lambda_i k\omega_i^2$, where λ_i is the ratio of torque to force. In the way that for clockwise rotating propellers, $\lambda_{2,3} = -\lambda$, whilst for counterclockwise propellers $\lambda_{1,4} = \lambda$.

Using vector-matrix notation, (1) is rewritable as follows:

$$M\dot{\zeta} + C(\zeta)\zeta = G + O(\zeta)\omega + E(\xi)\omega^2 + W(\zeta) + D(\zeta, \xi) \quad (16)$$

Where $\zeta = [\dot{X} \ \dot{Y} \ \dot{Z} \ p \ q \ r]^T$ is the generalized velocity vector and $\xi = [X \ Y \ Z \ \phi \ \theta \ \psi]^T$ is the position and the orientation of center of mass with respect to the inertial frame. M and $C(\zeta)$ are the inertia matrix and Coriolis-centripetal matrix, respectively.

$$M = \begin{bmatrix} mI_{3 \times 3} & 0_{3 \times 3} \\ 0_{3 \times 3} & diag(I_{xx}, I_{yy}, I_{zz}) \end{bmatrix} \quad (17)$$

$$C(\zeta) = \begin{bmatrix} 0 & 0 & 0 & 0 & 0 & 0 \\ 0 & 0 & 0 & 0 & 0 & 0 \\ 0 & 0 & 0 & 0 & 0 & 0 \\ 0 & 0 & 0 & 0 & I_{zz}r & -I_{yy}q \\ 0 & 0 & 0 & -I_{zz}r & 0 & I_{xx}p \\ 0 & 0 & 0 & I_{yy}q & -I_{xx}p & 0 \end{bmatrix} \quad (18)$$

, and in right-hand side of (16), terms G , $O(\zeta)\omega$, $E(\xi)\omega^2$, $W(\zeta)$, and $D(\zeta, \xi)$ are the gravity, gyroscopic, system actuator, lift and drag forces and moments, and external disturbances, respectively.

$$G = [0 \ 0 \ mg \ 0 \ 0 \ 0]^T \quad (19)$$

$$O(\zeta)\omega \quad (20)$$

$$= \left[\sum_{i=1}^4 \left(J_{prop} \left[\eta_i \Omega_b \times \begin{bmatrix} c_{\theta_i} \\ 0 \\ -s_{\theta_i} \end{bmatrix} \omega_i \right] \right) \right] \quad (21)$$

$$E(\xi)\omega^2 = \begin{bmatrix} R_{b2i} F_{thru} \\ M_{thru} \\ (c_\psi c_\theta c_{\theta_{tilt}} - (c_\phi s_\theta c_\psi + s_\phi s_\psi) s_{\theta_{tilt}}) k U_1 \\ (s_\psi c_\theta c_{\theta_{tilt}} - (c_\phi s_\theta s_\psi - s_\phi c_\psi) s_{\theta_{tilt}}) k U_1 \\ (-s_\theta c_{\theta_{tilt}} - c_\phi c_\theta s_{\theta_{tilt}}) k U_1 \\ s_{\theta_{tilt}} k l_s U_2 - c_{\theta_{tilt}} k \lambda U_3 \\ s_{\theta_{tilt}} k l_l U_4 \\ c_{\theta_{tilt}} k l_s U_2 + s_{\theta_{tilt}} k \lambda U_3 \end{bmatrix}$$

, where $U_1 = (u_1 + u_2 + u_3 + u_4)$, $U_2 = (u_1 - u_2 + u_3 - u_4)$, $U_3 = (u_1 - u_2 - u_3 + u_4)$ and $U_4 = (u_1 + u_2 - u_3 - u_4)$.

$$W(\zeta) = \begin{bmatrix} F_{aero_x} \\ F_{aero_y} \\ F_{aero_z} \\ M_{aero_x} \\ M_{aero_y} \\ M_{aero_z} \end{bmatrix} \quad (22)$$

$$= \begin{bmatrix} F_{D_1} + F_{D_2} + F_{D_3} + F_{D_4} \\ 0 \\ R_{b2i} \begin{bmatrix} F_{L_1} + F_{L_2} + F_{L_3} + F_{L_4} \\ 0 \\ l_l (F_{L_1} + F_{L_2} - F_{L_3} - F_{L_4}) \end{bmatrix} \\ 0 \end{bmatrix}$$

To simplify, all tilt angles are assumed to be equal to $(\theta_1 = \theta_2 = \theta_3 = \theta_4 = \theta_{tilt})$. Control commands $u_{1,2,3,4}$ used in (21) are clearly written as:

$$[u_1 \ u_2 \ u_3 \ u_4]^T = \begin{bmatrix} \omega_1^2 \\ \omega_2^2 \\ \omega_3^2 \\ \omega_4^2 \end{bmatrix} \quad (23)$$

Finally, the full dynamical model of the vehicle can be expressed as follows:

$$\dot{p} = f_1 + g_1 U_2 - g'_1 U_3 \quad (24a)$$

$$\dot{q} = f_2 + g_2 U_4 \quad (24b)$$

$$\dot{r} = f_3 + g_3 U_2 + g'_3 U_3 \quad (24c)$$

$$\dot{\phi} = p + q(s_\phi t_\theta) + r(c_\phi t_\theta) \quad (24d)$$

$$\dot{\theta} = qc_\phi - rs_\phi \quad (24e)$$

$$\dot{\psi} = q \left(s_\phi \frac{1}{c_\theta} \right) + r \left(c_\phi \frac{1}{c_\theta} \right) \quad (24f)$$

$$\dot{X} = f_4 + g_4 U_1 \quad (24g)$$

$$\dot{Y} = f_5 + g_5 U_1 \quad (24h)$$

$$\dot{Z} = f_6 + g_6 U_1 \quad (24i)$$

Where

$$f_1 = \frac{1}{I_{xx}} [(I_{yy} - I_{zz})qr - J_{prop}qs_{\theta_{tilt}}\omega_p] \quad (24a)$$

$$g_1 = \frac{k}{I_{xx}} [l_s s_{\theta_{tilt}}] \quad (24b)$$

$$g'_1 = \frac{k}{I_{xx}} [\lambda c_{\theta_{tilt}}] \quad (24c)$$

$$f_2 = \frac{1}{I_{yy}} [(I_{zz} - I_{xx})pr + J_{prop}(ps_{\theta_{tilt}} + rc_{\theta_{tilt}})\omega_p + M_{aero_y}] \quad (24d)$$

$$g_2 = \frac{k}{I_{yy}} [l_l s_{\theta_{tilt}}] \quad (24e)$$

$$f_3 = \frac{1}{I_{zz}} [(I_{xx} - I_{yy})pq - J_{prop} q c_{\theta_{tilt}} \omega_p] \quad (24f)$$

$$g_3 = \frac{k}{I_{zz}} [l_s c_{\theta_{tilt}}] \quad (24g)$$

$$g'_3 = \frac{k}{I_{zz}} [\lambda s_{\theta_{tilt}}] \quad (24h)$$

$$f_4 = \frac{1}{m} F_{aero_x} \quad (24i)$$

$$g_4 = \frac{k}{m} [c_{\psi} c_{\theta} c_{\theta_{tilt}} - (c_{\phi} s_{\theta} c_{\psi} + s_{\phi} s_{\psi}) s_{\theta_{tilt}}] \quad (24j)$$

$$f_5 = \frac{1}{m} F_{aero_y} \quad (24k)$$

$$g_5 = \frac{k}{m} [s_{\psi} c_{\theta} c_{\theta_{tilt}} - (c_{\phi} s_{\theta} s_{\psi} - s_{\phi} c_{\psi}) s_{\theta_{tilt}}] \quad (24l)$$

$$f_6 = \frac{1}{m} [mg + F_{aero_z}] \quad (24m)$$

$$g_6 = \frac{k}{m} [-s_{\theta} c_{\theta_{tilt}} - c_{\phi} c_{\theta} s_{\theta_{tilt}}] \quad (24n)$$

Where t_0 is $\tan()$ and $\omega_p = \omega_1 - \omega_2 - \omega_3 + \omega_4$.

Table 1: Nominal modeling parameters [25].

Symbol	Description	Magnitude
m_0	Mass	4.5 kg
l_{s_0}	Rotor distance to cog along y axis	0.3 m
l_{l_0}	Rotor distance to cog along y axis	0.3 m
I_{xx_0}	Moment of inertia along x axis	0.405 kg m ²
I_{yy_0}	Moment of inertia along y axis	0.405 kg m ²
I_{zz_0}	Moment of inertia along z axis	0.72 kg m ²
λ_0	Torque/force ratio	0.01 Nm/N
k_0	Motor thrust constant	4.8 × 10 ⁻⁵

Controller Design

The control design problem is to choose a control vector $[u_1 \ u_2 \ u_3 \ u_4]^T = [\omega_1^2 \ \omega_2^2 \ \omega_3^2 \ \omega_4^2]^T$ that compels the position

and the attitude to track some desired commanded values in order to stabilize and accomplish a mission in the presence of parametric uncertainty. The tracking control problem can be achieved by keeping the system trajectory on the sliding surface $S(t) = 0$ [43]. The integral type sliding surface S is selected as

$$S(t) = \left(\frac{d}{dt} + \lambda_c \right)^n \left(\int_0^t e \, dt \right) \quad (26)$$

, where λ_c is a strictly positive constant that defines the bandwidth of the error dynamics and n is the order of differential equation. The sliding surface $S(t) = 0$ represents a linear differential equation whose solution implies

$$\int e(t)$$

The integral of tracking errors are used to cancel the steady-state errors [43]. In this paper, the development and the stability analysis of the controller do not use any linearization.

In order to control and to stabilize the attitude and altitude, with respect to (24), the states that must be controlled to track desired values Z_d, p_d, q_d and r_d are $[Z \ p \ q \ r]^T$. So, the sliding surfaces are defined by

$$\begin{aligned} S_1 &= \dot{e}_z(t) + 2\lambda_{c_1} e_z(t) + \lambda_{c_1}^2 \int e_z(t) dt \\ S_2 &= e_p(t) + \lambda_{c_2} \int e_p(t) dt \\ S_3 &= e_q(t) + \lambda_{c_3} \int e_q(t) dt \\ S_4 &= e_r(t) + \lambda_{c_4} \int e_r(t) dt \end{aligned} \quad (27)$$

Where

$$\begin{aligned} e_z &= Z - Z_d \\ e_p &= p - p_d \\ e_q &= q - q_d \\ e_r &= r - r_d \end{aligned} \quad (28)$$

It is worth noting that, the desired angular velocities (p_d, q_d, r_d) are generated in controller by using the time derivative of the attitude angles and the velocity transformation matrix [25] and are defined as

$$\mathbb{E} = \begin{bmatrix} 1 & 0 & -s_{\theta} \\ 0 & c_{\phi} & s_{\phi} c_{\theta} \\ 0 & -s_{\phi} & c_{\phi} c_{\theta} \end{bmatrix} \quad (29)$$

$$[p_d \ q_d \ r_d]^T = \mathbb{E} \cdot \begin{bmatrix} \dot{\phi}_d \\ \dot{\theta}_d \\ \dot{\psi}_d \end{bmatrix} \quad (30)$$

From equation (27) the derivatives of S are determined as

$$\dot{S}_1 = \ddot{e}_z(t) + 2\lambda_{c_1} \dot{e}_z(t) + \lambda_{c_1}^2 e_z(t) \quad (31)$$

$$\dot{S}_4 = \dot{e}_r(t) + \lambda_{c_4} e_r(t)$$

By using (28), (24), and (25) and substituting them into (31), the equations become

$$\dot{S}_1 = -\ddot{Z}_d + f_6 + 2\lambda_{c_1} \dot{e}_z(t) + \lambda_{c_1}^2 e_z(t) + g_6 U_1 \quad (32a)$$

$$\dot{S}_2 = -\dot{p}_d + f_1 + \lambda_{c_2} e_p(t) + g_1 U_2 - g_1' U_3 \quad (32b)$$

$$\dot{S}_3 = -\dot{q}_d + f_2 + \lambda_{c_3} e_q(t) + g_2 U_4 \quad (32c)$$

$$\dot{S}_4 = -\dot{r}_d + f_3 + \lambda_{c_4} e_r(t) + g_3 U_2 + g_3' U_3 \quad (32d)$$

, which can be written as a vector form

$$\begin{bmatrix} \dot{S}_1 \\ \dot{S}_2 \\ \dot{S}_3 \\ \dot{S}_4 \end{bmatrix} = \begin{bmatrix} v_1 \\ v_2 \\ v_3 \\ v_4 \end{bmatrix} + \begin{bmatrix} g_6 & g_6 & g_6 & g_6 \\ g_1 - g_1' & -g_1 + g_1' & g_1 + g_1' & -g_1 - g_1' \\ g_2 & g_2 & -g_2 & -g_2 \\ g_3 + g_3' & g_3 + g_3' & g_3 + g_3' & g_3 + g_3' \end{bmatrix} \begin{bmatrix} u_1 \\ u_2 \\ u_3 \\ u_4 \end{bmatrix} \quad (33)$$

Where

$$\begin{aligned} v_1 &= -\ddot{Z}_d + f_6 + 2\lambda_{c_1} \dot{e}_z(t) + \lambda_{c_1}^2 e_z(t) \\ v_2 &= -\dot{p}_d + f_1 + \lambda_{c_2} e_p(t) \\ v_3 &= -\dot{q}_d + f_2 + \lambda_{c_3} e_q(t) \\ v_4 &= -\dot{r}_d + f_3 + \lambda_{c_4} e_r(t) \end{aligned} \quad (34)$$

To simplify, the equation (33) can be rewritten as a compact form:

$$\dot{S} = v + Gu \quad (35)$$

The purpose of keeping the scalar S at zero, it can now be achieved by choosing the control commands $[u_1 \ u_2 \ u_3 \ u_4]^T$ to satisfy the sliding condition equations [43]

$$\frac{1}{2} \frac{dS_i^2}{dt} \leq -\sigma_i |S_i|; \quad i = 1, 2, 3, 4 \quad (35)$$

, where σ_i ($i = 1, 2, 3, 4$), are strictly positive constants that can be chosen in order to set the desired reaching time to the sliding surfaces [44]. The equation (36) indicates that the squared distance to the surface, as measured by S^2 decreases along all system trajectories [43]. With respect to (36), it is tuned that

$$\begin{aligned} \sigma_1 &= \text{sgn}(S_1) \dot{S}_1 + 0.900 \\ \sigma_2 &= \text{sgn}(S_2) \dot{S}_2 + 0.037 \\ \sigma_3 &= \text{sgn}(S_3) \dot{S}_3 + 0.040 \\ \sigma_4 &= \text{sgn}(S_4) \dot{S}_4 + 0.008 \end{aligned} \quad (37)$$

By using (35), the controller which satisfies the sliding conditions (36) can be define as

$$u = G^{-1}[-v - \sigma \text{sgn}(S)] \quad (38)$$

, where G is assumed to be invertible. This control law can be considered as two parts as equivalent control that be shown as $G^{-1}[-v]$, which guarantees $\dot{S} = 0$, for the nominal model, and the other term defined as $G^{-1}[-\sigma \text{sgn}(S)]$, handles parameter uncertainties and disturbances. It is important to stress that in the presence of modeling imprecision, the control law becomes discontinuous and this leads to chattering. The chattering is undesirable since it involves high control action and may excite high-frequency dynamics that are neglected in the modeling. Thus, it must be eliminated by smoothing out the controller discontinuity in a thin boundary layer neighboring the switching surface [43]. This can be achieved by defining the thin boundary layers of widths Φ around the sliding surfaces. Therefore, replacing $\text{sgn}(S)$ with continuous saturation functions $\text{sat}(\frac{S}{\Phi})$. So, the equation (38) can be rewritten as:

$$u = G^{-1} \left[-v - \sigma \text{sat}\left(\frac{S}{\Phi}\right) \right] \quad (39)$$

The parameter uncertainties are modeled by an additive variance Δ to the nominal values, used for controlling development. To illustrate this modeling imprecision, only a limited number of uncertainties are considered [45].

$$m = m_0(1 + \Delta m) \quad (40a)$$

$$I_{xx} = I_{xx_0}(1 + \Delta I_{xx}) \quad (40b)$$

$$I_{yy} = I_{yy_0}(1 + \Delta I_{yy}) \quad (40c)$$

$$I_{zz} = I_{zz_0}(1 + \Delta I_{zz}) \quad (40d)$$

, where the nominal values are illustrated in Table 1, and the additive uncertainties values are taken as follow

$$|\Delta m| \leq 0.1 \quad (41a)$$

$$|\Delta I_{xx}| \leq 0.2 \quad (41b)$$

$$|\Delta I_{yy}| \leq 0.2 \quad (41c)$$

$$|\Delta I_{zz}| \leq 0.2 \quad (41d)$$

Finally, the control law considering the parameter uncertainties can be defined as

$$\begin{bmatrix} u_1 \\ u_2 \\ u_3 \\ u_4 \end{bmatrix} = (G + G\Delta G)^{-1} \begin{bmatrix} -(v_1 + f_6\Delta f_6) - \sigma_1 \text{sat}\left(\frac{S_1}{\Phi_1}\right) \\ -(v_2 + f_1\Delta f_1) - \sigma_2 \text{sat}\left(\frac{S_2}{\Phi_2}\right) \\ -(v_3 + f_2\Delta f_2) - \sigma_3 \text{sat}\left(\frac{S_3}{\Phi_3}\right) \\ -(v_4 + f_3\Delta f_3) - \sigma_4 \text{sat}\left(\frac{S_4}{\Phi_4}\right) \end{bmatrix} \quad (42)$$

so, the compact form is

$$u = \hat{G}^{-1} \left[-\hat{v} - \sigma \text{sat}\left(\frac{S}{\Phi}\right) \right] \quad (43)$$

that ΔG and Δf_i ($i = 6, 1, 2, 3$), are created due to uncertainties (40), which are applied on f and g (25), in control design. Also, \hat{G} and \hat{v} , are chosen estimated of G and v , respectively.

For verification of the proposed nonlinear controller, a linear based controller is designed and considered for comparison. For developing the linear based controller, it is assumed that in the set of equations (24)

$$\phi \approx 0 \quad (44a)$$

$$\theta \approx 0 \quad (44b)$$

$$\psi \approx 0 \quad (44c)$$

$$\dot{p} \approx \ddot{\phi} \quad (44d)$$

$$\dot{q} \approx \ddot{\theta} \quad (44e)$$

$$\dot{r} \approx \ddot{\psi} \quad (44f)$$

then, the control law is redesigned and simulation results are compared with the proposed controller.

Simulation Results

The performance of the sliding mode controller is evaluated on the nonlinear dynamic model of the tilt-wing UAV in MATLAB/Simulink. It should be recalled that the desired commands in these simulations are filtered by a low-pass filter because they are subjected to derivation in the process of controller development and it is achieved by smoothing the command signals.

Also, the sliding boundary layers Φ_i are tuned as 0.01 for all surfaces. Starting with all zero initial configurations of the UAV. Additionally, the tilt angles for all wings are selected as $\Theta_{tilt} = \frac{\pi}{2}$ during the flight mission. With this assumption, aerodynamics moments are equal to zero.

The sliding mode control conducted really well in tracking the reference command inputs. Figure 4 and Figure 5 illustrate the response of sliding mode controller to track the desired altitude and attitude

commands signal, respectively. These figures show that the proposed controller handled the tracking of command signals in appropriate time length in the presence of uncertainties. Note that, Figure 6 and Figure 7 show the control errors and the control efforts of the controller defined as square of rotors rotation, respectively. From the tracking error figure it can be inferred that the controller response is acceptable.

It is significant to emphasize that the control effort is small enough and the magnitude of the motor forces that need to be generated do not overcome the physical limits (≈ 16 N) of the rotors [21] (see Figure 8). To illustrate that the sliding surfaces tend to zero, its values are shown during the simulation in Figure 9.

In this paper, there are no control efforts on X and Y direction of the vehicle. Figure 10 shows the 3D trajectory of UAV's center of mass. In Figure 11 time-history of accelerations are shown. Results illustrate that linear and angular accelerations are in an acceptable range. The Figure 12 is given to show the values of linear and angular velocities during the simulation. Also, the need to use a controller based on a nonlinear system is illustrated in Figures 13 and 14 with comparison of sensitivity of controllers in the presence of pitch noise (Figure 15) and pitch moment disturbance (Figure 16).

Conclusion and Future Works

In this paper, a MIMO integral type sliding mode controller is developed in several stages for the nonlinear model of the tilt-wing UAV that can take-off and land vertically. This controller is able to deal with parameter uncertainties due to modeling imprecision. It is necessary to mention that in development of the controller, there is no linearization. Simulations conducted show that the controller has good tracking performance and robustness in the presence of uncertainties.

We have indicated our work on controller design on a new tilt-wing aerial vehicle. Future works will incorporate advances and improvements on the controller in combination with adaptation. Additionally, the effects of tilt angle of wing and the uncertainty it produces will be analyzed.

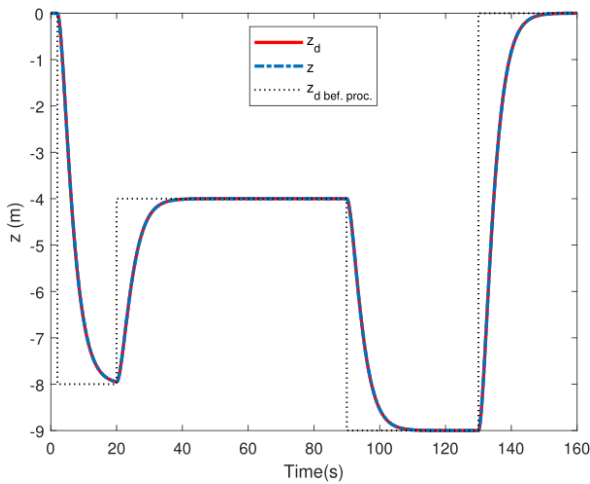


Figure 4: Altitude Control Using Sliding Mode Controller.

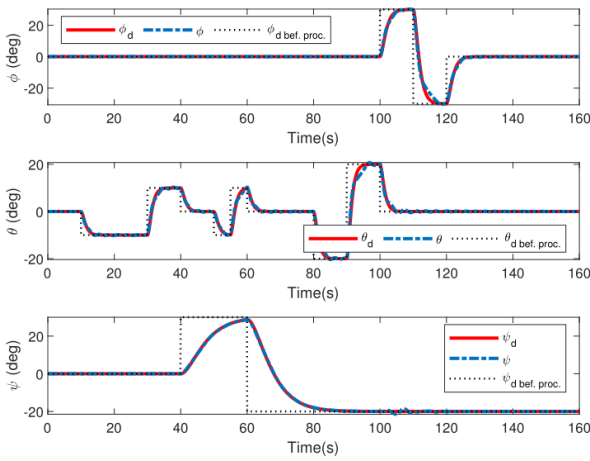


Figure 5: Attitude Control Using Sliding Mode Controller.

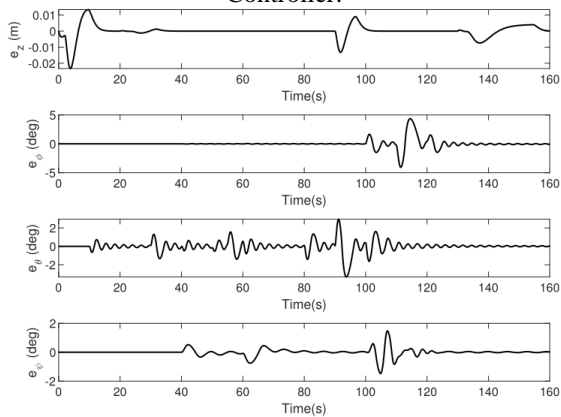


Figure 6: Tracking Errors Using Sliding Mode Controller.

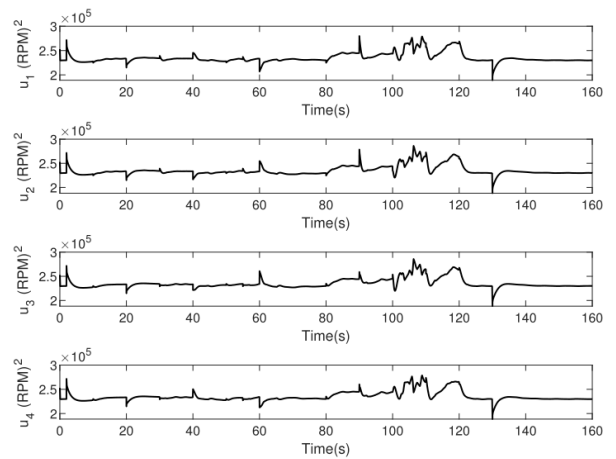


Figure 7: Control Effort in Sliding Mode Controller.

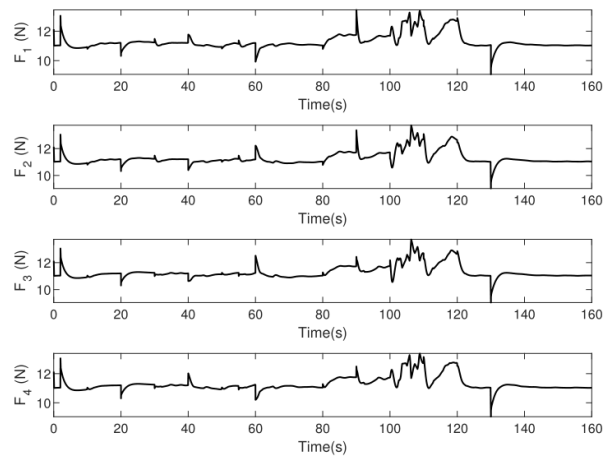


Figure 8: Forces Generated by the Motors.

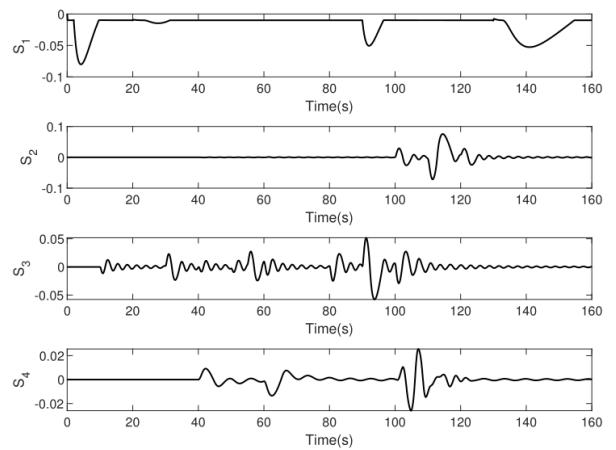


Figure 9: Surfaces values during simulation.

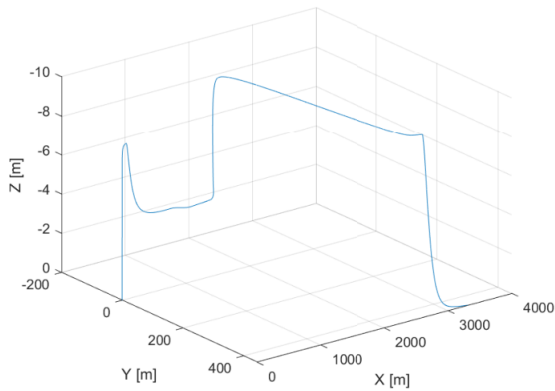


Figure 10: 3D Trajectory of the Vehicle Center of Mass.

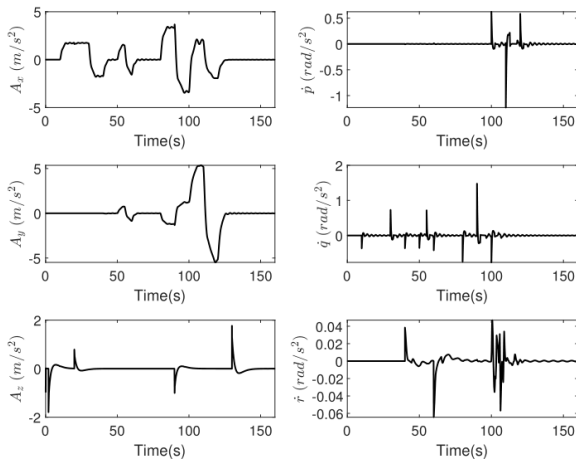


Figure 11: Linear and Angular Accelerations.

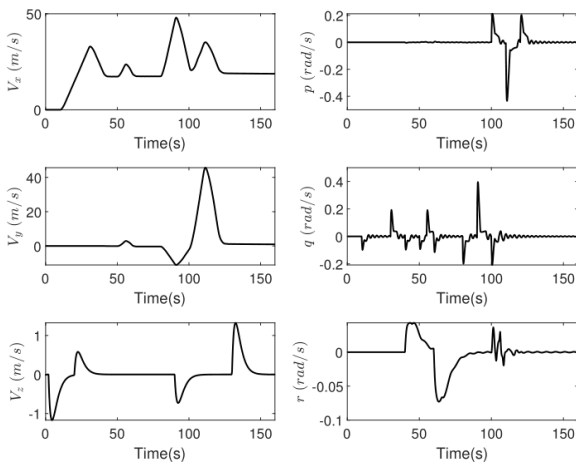


Figure 12: Linear and Angular Velocities.

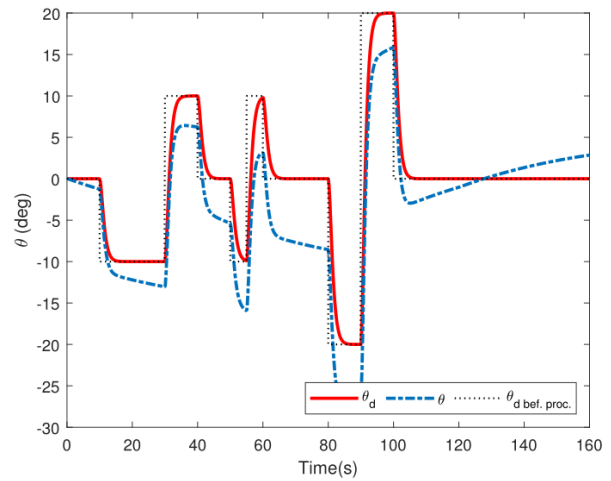


Figure 13: Pitch Control Using Sliding Mode Controller Based on Linear Dynamics in the Presence of Noise and Disturbance.

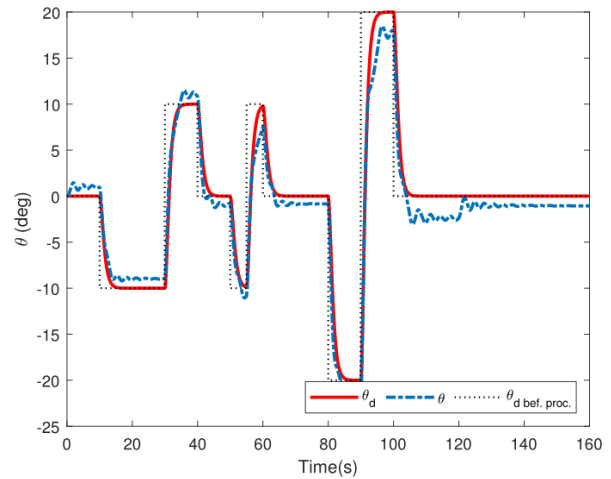


Figure 14: Pitch Control Using Sliding Mode Controller Based on nonlinear Dynamics in the Presence of Noise and Disturbance.

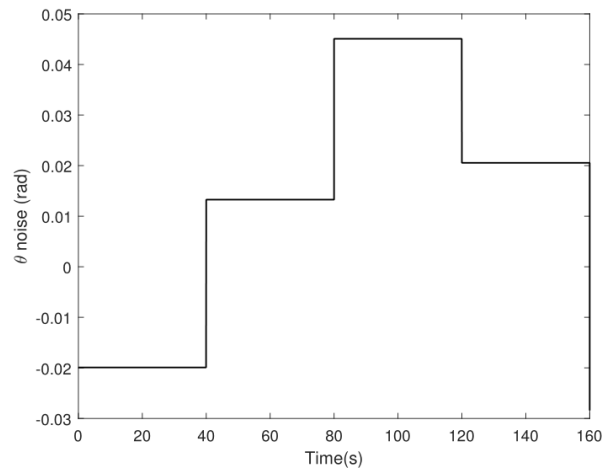


Figure 15: Pitch Angle Noise.

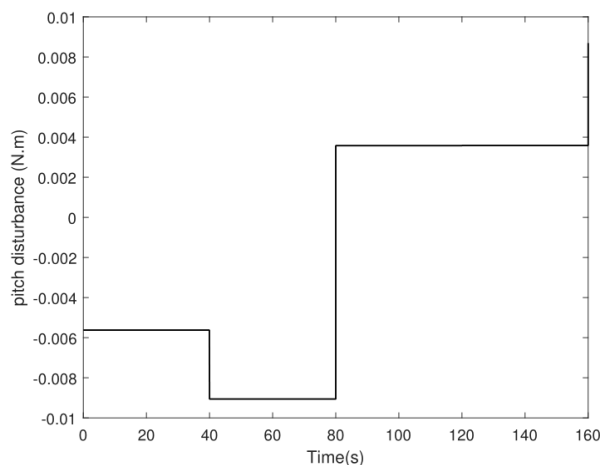


Figure 16: Pitch Moment Disturbance.

References

- [1] A. C. Watts, V. G. Ambrosia, and E. A. Hinkley, "Unmanned aircraft systems in remote sensing and scientific research: Classification and considerations of use," *Remote Sens.*, vol. 4, no. 6, pp. 1671–1692, 2012, doi: 10.3390/rs4061671.
- [2] L. Marin, "The Humanitarian Drone and the Borders: Unveiling the Rationales Underlying the Deployment of Drones in Border Surveillance.," *Futur. Drone Use*, vol. 27, pp. 4–20, 2016, doi: 10.1007/978-94-6265-132-6.
- [3] S. Srinivasan, H. Latchman, J. Shea, T. Wong, and J. McNair, "Airborne traffic surveillance systems - Video surveillance of highway traffic," *VSSN'04 - Proc. ACM Second Int. Work. Video Sureveillance Sens. Networks*, pp. 131–135, 2004.
- [4] R. U. Remotely, "Monitoring system for power lines and right-of-way using remotely piloted drone," no. 19, 1987.
- [5] A. A. Obaidi, "Drone-based personal delivery system," *US Pat. App. 14/869,922*, vol. 2022, no. 19, pp. 2015–2018, 2017.
- [6] H. Gu, X. Lyu, Z. Li, S. Shen, and F. Zhang, "Development and experimental verification of a hybrid vertical take-off and landing (VTOL) unmanned aerial vehicle(UAV)," *2017 Int. Conf. Unmanned Aircr. Syst. ICUAS 2017*, pp. 160–169, 2017, doi: 10.1109/ICUAS.2017.7991420.
- [7] B. Yan, P. Dai, R. Liu, M. Xing, and S. Liu, "Adaptive super-twisting sliding mode control of variable sweep morphing aircraft," *Aerosp. Sci. Technol.*, vol. 92, pp. 198–210, 2019, doi: 10.1016/j.ast.2019.05.063.
- [8] I. Mir, A. Maqsood, S. A. Eisa, H. Taha, and S. Akhtar, "Optimal morphing – augmented dynamic soaring maneuvers for unmanned air vehicle capable of span and sweep morphologies," *Aerosp. Sci. Technol.*, vol. 79, pp. 17–36, 2018, doi: 10.1016/j.ast.2018.05.024.
- [9] D. Xu, Z. Hui, Y. Liu, and G. Chen, "Morphing control of a new bionic morphing UAV with deep reinforcement learning," *Aerosp. Sci. Technol.*, vol. 92, no. May, pp. 232–243, 2019, doi: 10.1016/j.ast.2019.05.058.
- [10] M. Wu, Z. Shi, T. Xiao, and H. Ang, "Energy optimization and investigation for Z-shaped sun-tracking morphing-wing solar-powered UAV," *Aerosp. Sci. Technol.*, vol. 91, pp. 1–11, 2019, doi: 10.1016/j.ast.2019.05.013.
- [11] A. K. Jha and J. N. Kudva, "Morphing aircraft concepts, classifications, and challenges," *Smart Struct. Mater. 2004 Ind. Commer. Appl. Smart Struct. Technol.*, vol. 5388, p. 213, 2004, doi: 10.1117/12.544212.
- [12] Y. Wang, Y. Zhou, and C. Lin, "Modeling and control for the mode transition of a novel tilt-wing UAV," *Aerosp. Sci. Technol.*, vol. 91, pp. 593–606, 2019, doi: 10.1016/j.ast.2019.05.046.
- [13] G. Sanchez, R. D. Salazar, M. Hassanalian, and B. Abdelkefi, "Sizing and performance analysis of albatross-inspired tilt-wing unmanned air vehicle," *AIAA/ASCE/AHS/ASC Struct. Struct. Dyn. Mater. Conf. 2018*, no. 210049, pp. 1–11, 2018, doi: 10.2514/6.2018-1445.
- [14] J. J. Dickeson *et al.*, " ∞ Hover-To-Cruise Conversion for a Tilt-Wing Rotorcraft," *Proc. 44th IEEE Conf. Decis. Control. Eur. Control Conf. CDC-ECC '05*, vol. 2005, pp. 6486–6491, 2005, doi: 10.1109/CDC.2005.1583202.
- [15] S. Kim, S. Yoon, and J. Suk, "Neural Network Controller Design for a Single Tilt-Wing UAV," vol. 00, p. 2014, 2014.
- [16] A. Lindqvist, E. Fresk, and G. Nikolakopoulos, "Optimal design and modeling of a tilt wing aircraft," *2015 23rd Mediterr. Conf. Control Autom. MED 2015 - Conf. Proc.*, pp. 701–708, 2015, doi: 10.1109/MED.2015.7158828.
- [17] R. Whittle, "Air mobility bonanza beckons electric VTOL developers," *Vertiflite*, vol. 63, no. 2, pp. 14–21, 2017.
- [18] E. Cetinsoy, C. Hancer, K. T. Oner, E. Sirimoglu, and M. Unel, "Aerodynamic design and characterization of a quad tilt-wing UAV via wind tunnel tests," *Journal of Aerospace Engineering*, vol. 25, no. 4, 2012, doi: 10.1061/(ASCE)AS.1943-5525.0000161.
- [19] K. Muraoka, N. Okada, and D. Kubo, "Quad tilt wing VTOL UAV: Aerodynamic characteristics and prototype flight test," *AIAA Infotech Aerosp. Conf. Exhib. AIAA Unmanned...Unlimited Conf.*, no. April, pp. 6–13, 2009.
- [20] S. SUZUKI *et al.*, "Attitude Control of Quad Rotors QTW-UAV with Tilt Wing Mechanism," *J. Syst. Des. Dyn.*, vol. 4, no. 3, pp. 416–428, 2010, doi: 10.1299/jsdd.4.416.
- [21] K. T. Oner, E. Cetinsoy, E. Sirimoglu, C. Hancer, T. Ayken, and M. Unel, "LQR and SMC stabilization of a new unmanned aerial vehicle," *World Acad. Sci. Eng. Technol.*, vol. 58, pp. 373–378, 2009.
- [22] C. Hancer, K. T. Oner, E. Sirimoglu, E. Cetinsoy, and M. Unel, "Robust hovering control of a quad tilt-wing UAV," *IECON Proc. (Industrial Electron. Conf.)*, pp. 1615–1620, 2010, doi: 10.1109/IECON.2010.5675441.
- [23] C. Hancer, K. T. Oner, E. Sirimoglu, E. Cetinsoy, and M. Unel, "Robust position control of a tilt-wing quadrotor," *Proc. IEEE Conf. Decis. Control*, pp. 4908–4913, 2010, doi: 10.1109/CDC.2010.5717283.
- [24] E. Çetinsoy *et al.*, "Design and development of a tilt-wing UAV," *Turkish J. Electr. Eng. Comput. Sci.*, vol. 19, no. 5, pp. 733–741, 2011, doi: 10.3906/elk-1007-621.
- [25] E. Cetinsoy *et al.*, "Design and construction of a novel quad tilt-wing UAV," in *Mechatronics*, 2012, vol. 22, no. 6, pp. 723–745, doi: 10.1016/j.mechatronics.2012.03.003.
- [26] K. Taha öner *et al.*, "Mathematical modeling and vertical flight control of a tilt-wing UAV," *Turkish J.*

- Electr. Eng. Comput. Sci.*, vol. 20, no. 1, pp. 149–157, 2012, doi: 10.3906/elk-1007-624.
- [27] K. Muraoka, N. Okada, D. Kubo, and M. Daisuk, "Transition flight of quad tilt wing VTOL UAV," *28th Congr. Int. Counc. Aeronaut. Sci. 2012, ICAS 2012*, vol. 4, pp. 3242–3251, 2012.
- [28] M. Sato and K. Muraoka, "Flight test verification of flight controller for Quad Tilt Wing Unmanned Aerial Vehicle," *AIAA Guid. Navig. Control Conf.*, pp. 1–17, 2013.
- [29] M. Sato and K. Muraoka, "Flight controller design and demonstration of quad-tilt-wing unmanned aerial vehicle," *J. Propuls. Power*, vol. 31, no. 5, pp. 1071–1082, 2015, doi: 10.2514/1.G000263.
- [30] Y. Yildiz, M. Unel, and A. E. Demirel, "Adaptive nonlinear hierarchical control of a quad tilt-wing UAV," *2015 Eur. Control Conf. ECC 2015*, pp. 3623–3628, 2015, doi: 10.1109/ECC.2015.7331093.
- [31] Y. Yildiz, M. Unel, and A. E. Demirel, "Nonlinear hierarchical control of a quad tilt-wing UAV: An adaptive control approach," *Int. J. Adapt. Control Signal Process.*, vol. 31, no. 9, pp. 1245–1264, 2017, doi: 10.1002/acs.2759.
- [32] T. Mikami and K. Uchiyama, "Design of flight control system for quad tilt-wing UAV," *2015 Int. Conf. Unmanned Aircr. Syst. ICUAS 2015*, vol. 2, no. c, pp. 801–805, 2015, doi: 10.1109/ICUAS.2015.7152364.
- [33] H. Totoki, Y. Ochi, M. Sato, and K. Muraoka, "Design of gain scheduled stability and control augmentation system for Quad-Tilt-Wing UAV," *AIAA Guid. Navig. Control Conf. 2013*, no. January, pp. 6–13, 2015.
- [34] H. Totoki, Y. Ochi, M. Sato, and K. Muraoka, "Flight Testing of a Gain-Scheduled Stability and Control Augmentation System for a Quad-Tilt-Wing UAV," *AIAA Guid. Navig. Control Conf. 2013*, no. January, pp. 1–10, 2016, doi: 10.2514/6.2016-0084.
- [35] H. Totoki, Y. Ochi, M. Sato, and K. Muraoka, "Design and testing of a low-order flight control system for quad-tilt-Wing UAV," *J. Guid. Control. Dyn.*, vol. 39, no. 10, pp. 2423–2430, 2016, doi: 10.2514/1.G001577.
- [36] K. Benkhoud and S. Bouallegue, "Modeling and LQG Controller Design for a Quad Tilt-Wing UAV," *3rd Int. Conf. Autom. Control Eng. Comput. Sci. (ACECS); Proc. Eng. Technol.*, vol. 13, pp. 198–204, 2016.
- [37] K. Benkhoud and S. Bouallegue, "Model Predictive Control design for a convertible Quad Tilt-Wing UAV," *4th Int. Conf. Control Eng. Inf. Technol. CEIT 2016*, pp. 16–18, 2017, doi: 10.1109/CEIT.2016.7929042.
- [38] K. Benkhoud, S. Bouallegue, and M. Ayadi, "Rapid control prototyping of a quad-tilt-wing unmanned aerial vehicle," *2017 Int. Conf. Control. Autom. Diagnosis, ICCAD 2017*, pp. 423–428, 2017, doi: 10.1109/CADIAG.2017.8075696.
- [39] K. Ben Khoud, S. Bouallègue, and M. Ayadi, "Design and co-simulation of a fuzzy gain-scheduled PID controller based on particle swarm optimization algorithms for a quad tilt wing unmanned aerial vehicle," *Trans. Inst. Meas. Control*, vol. 40, no. 14, pp. 3933–3952, 2018, doi: 10.1177/0142331217740947.
- [40] K. Benkhoud and S. Bouallegue, "Dynamics modeling and advanced metaheuristics based LQG controller design for a Quad Tilt Wing UAV," *Int. J. Dyn. Control*, vol. 6, no. 2, pp. 630–651, 2018, doi: 10.1007/s40435-017-0325-7.
- [41] K. Masuda and K. Uchiyama, "Robust control design for Quad Tilt-Wing UAV," *Aerospace*, vol. 5, no. 1, 2018, doi: 10.3390/aerospace5010017.
- [42] K. Masuda and K. Uchiyama, "Flight Controller Design Using μ -synthesis for Quad Tilt-Wing UAV," no. January, pp. 1–25, 2019, doi: 10.2514/6.2019-1918.
- [43] J. E. Slotine and P. Hall, *Applied Nonlinear Control*.
- [44] M. Bahrami, J. Roshanian, and B. Ebrahimi, "Robust Integral Sliding-Mode Control of an Aerospace Launch Vehicle," *J. Aerosp. Sci. Technol.*, vol. 3, no. 3, pp. 143–149, 2006.
- [45] H. Xu, M. D. Mirmirani, and P. A. Ioannou, "Adaptive sliding mode control design for a hypersonic flight vehicle," *J. Guid. Control. Dyn.*, vol. 27, no. 5, pp. 829–838, 2004, doi: 10.2514/1.12596.

COPYRIGHTS

©2022 by the authors. Published by Iranian Aerospace Society This article is an open access article distributed under the terms and conditions of the Creative Commons Attribution 4.0 International (CC BY 4.0) (<https://creativecommons.org/licenses/by/4.0/>).

